Cellular/Molecular

Ca^{2+} Ion Permeability and Single-Channel Properties of the Metabotropic Slow EPSC of Rat Purkinje Neurons

Marco Canepari,[1] Céline Auger,[1,2] and David Ogden[1]

[1]National Institute for Medical Research, London NW7 1AA, United Kingdom, and [2]Laboratoire de Physiologie Cérébrale, Unité Mixte de Recherche 8118, Université Paris V, Paris 75006, France

The slow EPSC (sEPSC) of cerebellar parallel fiber → Purkinje neuron synapses is mediated by metabotropic glutamate receptor type 1 (mGluR1) activation of nonselective cation channels. Here, the channel properties were studied with uniform calibrated photorelease of L-glutamate with ionotropic receptors blocked, allowing isolation of postsynaptic processes, or with parallel fiber stimulation or mGluR1 agonist application. Evoked current and fluorescence from Ca^{2+} indicators were recorded. Noise analysis of the mGluR1 current gave a single-channel conductance of 0.6 pS and showed low open probability at maximal mGluR1 activation. Similar small single-channel conductances were obtained with the mGluR1 agonist (*S*)-dihydroxyphenylglycine, with parallel fiber or climbing fiber stimulation. The mGluR1 current fluctuations were unaffected by potassium channel blockers. Photoreleased L-glutamate triggered a Ca^{2+} concentration increase in the distal dendrites with a time course similar to that of the mGluR1 current. The proximal dendritic and somatic Ca^{2+} changes were delayed with respect to the current. Ca^{2+} channel blockers and the phospholipase Cβ inhibitor 1-[6-[((17β)-3-methoxyestra-1,3,5[10]-trien-17-yl)amino]hexyl]-1H-pyrrole-2,5-dione, which inhibits mGluR1-activated intracellular Ca^{2+} release, did not prevent the dendritic Ca^{2+} concentration increase. Polyamine naphthylacetyl spermine and cationic adamantanes that block the pore of the channel were used to vary the mGluR1 current over a wide range in each cell but still at maximal mGluR1 activation. The Ca^{2+} influx was inhibited in parallel with the current. The results show that the mGluR1-activated current and the sEPSC are attributable to small-conductance, low-open probability Ca^{2+}-permeable cation channels that will mediate spine-specific Ca^{2+} influx during the parallel fiber sEPSP.

Key words: **calcium; cerebellum; channel; EPSP; Purkinje cell; synaptic**

Introduction

Brief tetanic stimulation of parallel fibers (PFs) in the molecular layer of the cerebellar cortex produces a slow EPSP (sEPSP) or slow EPSC (sEPSC) in Purkinje neurons (PNs; Batchelor and Garthwaite, 1993, 1997; Tempia et al., 1998). The sEPSP is blocked by the metabotropic type 1 glutamate receptor (mGluR1) antagonists (*R*,*S*)-α-methyl-4-carboxyphenylglycine (MCPG) and 7-(hydroxymino)cyclopropa[b]cromen-1a-carboxylate ethyl ester and is produced by activation of a nonselective cation channel (Canepari et al., 2001b). The coupling of the sEPSC to mGluR1 activation is independent of phophoinositide metabolism (Hirono et al., 1998; Tempia et al., 1998; Canepari et al., 2001b) but requires a G-protein (Tempia et al., 1998; Canepari and Ogden, 2003) and is inhibited by tyrosine phosphorylation (Canepari and Ogden, 2003). Activation of mGluR1 after stimulation of PF has been associated with an increase of dendritic Ca^{2+} concentration. This has been attributed to release of Ca^{2+} ions from intracellular stores by D-myo-inositol-1,4,5-triphosphate ($InsP_3$; Takechi et al., 1998). However, voltage-gated Ca^{2+} channels activated by depolarization could contribute Ca^{2+} influx during the sEPSP. More importantly, there is the possibility of Ca^{2+} influx via the mGluR1-activated nonselective channel. This would happen in individual spines activated by tetanic PF stimulation during the sEPSC, producing a synapse-specific Ca^{2+} increase.

Two observations suggest a role of mGluR1 receptors in motor coordination: first, mGluR1α-deficient mice are ataxic and show developmental abnormalities in the innervation of PN (Aiba et al., 1994); and second, in clinical neoplastic cerebellar ataxia, the deficit in motor coordination has been shown to be associated with autoantibodies generated against mGluR1 (Sillevis-Smitt et al., 2000). The synaptic mechanism underlying cerebellar motor coordination is thought to be a long-term depression of parallel fiber synapses, which is linked to an increase in postsynaptic Ca^{2+} concentration. It is of interest to know the contribution to postsynaptic Ca^{2+} concentration changes that may be made by Ca^{2+} influx through the mGluR1-activated channel and the role this may play in PF → PN synaptic plasticity. Ca^{2+} influx through the mGluR1-activated channels themselves would have the property of restricting the Ca^{2+} increase to spines activated by tetanic PF activity, in contrast to the wider spread of action of $InsP_3$ (Finch and Augustine, 1998), which diffuses more rapidly intracellularly than Ca^{2+} (Allbritton et al., 1992).

In the experiments described here, the channel properties of

Received Dec. 5, 2003; revised Feb. 4, 2004; accepted Feb. 21, 2004.

We thank John Corrie and George Papageorgiou (National Institute for Medical Research) for providing NI- and MNI-caged L-glutamate and for advice and discussion and Dr. L. Magazanik and Dr. V. Gmiro (Sechenov Institute of Evolutionary Physiology and Biochemistry, St. Petersburg), for kindly providing IEM1460.

Correspondence should be addressed to David Ogden, Department of Neurophysiology, National Institute for Medical Research, The Ridgeway, London, NW7 1AA, UK. E-mail: dogden@nimr.mrc.ac.uk.

DOI:10.1523/JNEUROSCI.5374-03.2004

 0270-6474/04/243563-11$15.00/0

the PF and climbing fiber (CF) sEPSC were investigated with nerve stimulation, with quantitative photolytic release of L-glutamate from 7-nitroindolinyl (NI)-caged or 4-methoxy-7-nitroindolinyl (MNI)-caged glutamate, or with bath application of the mGluR1 agonist (*S*)-dihydroxyphenylglycine (DHPG). The photolytic release of L-glutamate permitted pharmacological manipulation of Ca^{2+} influx through voltage-gated and mGluR1-activated channels without the problems of interfering with presynaptic processes. The results show a Ca^{2+}-permeable nonselective cation channel of small unitary conductance and low maximum open probability.

Materials and Methods

Wistar rats, 19–22 d old or as specified, were killed by cervical dislocation and decapitated; the brain was removed to iced saline; and parasagittal slices 200 μm thick or transverse slices 300 or 350 μm thick were cut from the cerebellum. Slices were viewed with a Zeiss (Oberkochen Germany) Axioskop 1FS microscope, a Leica (Nussloch, Germany) 63 × 0.9w objective, and, to avoid untimely photolysis, 550/40 nm bandpass illumination. A xenon arc flashlamp filtered at 290–370 nm (UG11; Schott, Mainz, Germany) was focused into the slice from below via a Reichert (Nussloch, Germany) silica condenser (0.9 numerical aperture), illuminating a spot 200 μm in diameter. The arc image was aligned and focused in the specimen plane, and calibration of photolytic conversion per flash was made as described by Canepari et al. (2001a) for the NI- and MNI-caged glutamate. Unless specified, photolysis experiments were done using the MNI-caged glutamate. Transmission at 320 nm through 200 μm slices from 20-d-old rats was measured as 0.42 ± 0.07 (SD) in the molecular layer and 0.36 ± 0.08 in the granule cell layer. Flashlamp intensity was set to maximum, converting in the molecular layer 32% MNI-caged glutamate after correction for attenuation in the slice. Lower L-glutamate concentrations were produced by reducing flash intensity with calibrated neutral density filters in the photolysis light path.

Solutions. In photolysis and DHPG application experiments, external saline contained (in mM): 135 NaCl, 4 KCl, 2 $MgSO_4$ or $MgCl_2$, 2 $CaCl_2$, 2 $NaHCO_3$, 25 glucose, and 10 HEPES-Na, pH 7.3 (305 mOsm/kg); experiments were made at 32°C, and a continuous stream of hydrated O_2/0.5% CO_2 was blown over the solution surface. To isolate the mGluR1-evoked current, experiments were done with ionotropic glutamate receptor antagonists 2,3-dioxo-6-nitro-1,2,3,4-tetrahydrobenzo[f]quinoxaline-7-sulfonamide (NBQX, 50–100 μM) and 2-amino-5-phosphonopentanoic acid (AP-5, 50 μM), with the $GABA_A$ receptor antagonist bicuculline (20 μM) and with the voltage-gated sodium channel blocker Tetrodotoxin (TTX, 1 μM). Caged glutamate and drugs were applied in static 1 ml of solution. For PF stimulation experiments in transverse slices and CF stimulation in sagittal slices, the solution contained (in mM): 125 NaCl, 3 KCl, 1 $MgSO_4$, 2 $CaCl_2$, 25 $NaHCO_3$, and 25 glucose gassed with 5% CO_2 in O_2. Whole-cell recordings were with an Axoclamp 2A or Axopatch 200A and 2.5 MΩ pipettes filled with the following internal solution (in mM): 110 K gluconate, 50 HEPES, 10 KCl, 4 $MgSO_4$, 4 Na_2ATP, 10 creatine phosphate, and 0.05 GTP, pH 7.3, with KOH. Potentials were corrected for the junction potential of 12 mV pipette negative between this solution and the external solution. Series resistance was monitored at 5 min intervals, and experiments in which it increased to >12 MΩ or in which the leak current at –75 mV exceeded –0.5 nA were discontinued.

Data were collected with Spike 2 (Cambridge Electronic Design, Cambridge, UK) or WinWCP (Dr J. Dempster, University of Strathclyde, Glasgow, UK) in a CED1401+ or Power 1401 interface (Cambridge Electronic Design; sampled at 10 kHz; low-pass filter, 2 kHz; −3 dB). Data were analyzed in IgorPro (Wavemetrics). Voltage pulses of −5 mV were applied to the pipette at the beginning of each cell to assess the effects of loss of voltage clamp and filtering of dendritic signals. The evoked current was fitted with the predictions of a two-compartment model taking into account series resistances from pipette to soma and from soma to dendritic compartment and parallel capacitance and membrane resistance from soma and dendrite compartments to bath (Llano et al., 1991; Roth and Hausser, 2001). The series resistances from pipette to soma and soma to dendrites were used to calculate the voltage escape, assuming current arose entirely in the dendritic compartment. For cable analysis, data were sampled at 250 kHz; low-pass filter, 50 kHz (3 dB).

Chemicals were Analar grade (BDH, Poole, UK), and biochemicals and drugs were obtained from Sigma (Poole, UK), Tocris (Bristol, UK), or Research Biochemicals (Poole, UK). Experiments with the Ca^{2+} channel blocker agatoxin IVA (AGA4A; Peptide Institute, Osaka, Japan) were done with 0.1 mg/ml cytochrome *c* present to avoid unspecific binding.

MNI- and NI-caged L-glutamate were synthesized, purified, and kindly provided by John Corrie and George Papageorgiou (National Institute for Medical Research, London, UK). At a 1 mM concentration, these reagents, the photolytic intermediates, and byproducts have been shown to have no pharmacological activity on glutamate receptors or synaptic transmission (Canepari et al., 2001a). Near UV transmission through the slice was measured separately at 320 nm or by direct measurement during the experiment with a bolometer (Rapp Optoelectronic, Germany) mounted in the microscope.

Fluorescence imaging. For initial Ca^{2+} imaging experiments, fluo-4 (500 μM; Molecular Probes, Eugene, OR) was included in the internal solution. Fluorescence epi-illumination was at 470 nm, and emission images at 520–650 nm were collected continuously by a Hamamatsu (Shizuoka-Ken, Japan) 4880–82 CCD camera (1 μm pixel size with 4 × 4 binning, 10 bit) with 19 or 38 msec exposures. Images were analyzed in Matlab (The Mathworks, Natick, MA), and fluorescence changes in each binned pixel were expressed as $\Delta F/F$ relative to the average level in 10 frames before the flash. For analysis, each PN was subdivided into regions in the distal dendrites (>100 μm from the soma), proximal dendrites, and soma.

A quantitative estimate of Ca^{2+} flux was obtained with an internal solution containing a high concentration of bis-fura-2 (1 mM; K_d, 370 nM; Molecular Probes) and 100 μM $CaCl_2$, giving high buffering capacity of the indicator and setting free Ca^{2+} concentration at 30 nM. Fluorescence was excited at 420 nm, and emitted light was recorded at 560 ± 80 nm with an intensified CCD camera (I-Pentamax; Princeton Instruments Inc., Trenton, NJ) or a photomultiplier (PMT; H7422; Hamamatsu) shuttered to avoid saturation during the flash. CCD images of 256 × 256 pixels (1 pixel ~ 1 μm^2 in the image) were acquired at an interframe interval of 35 msec. In PMT recordings, light was detected from a 50-μm-diameter circular region that could be moved on the image, usually in the distal dendrite. The signal was filtered at 160 Hz, acquired at 1 kHz, and digitally low-pass-filtered at 100 Hz.

Photolysis of MNI-caged glutamate releases 4-methoxy-7-nitrosoindole as a byproduct, and this strongly absorbs 420 nm light (Papageorgiou and Corrie, 2000), decreasing excitation of bis-fura-2 fluorescence after the flash. When necessary, recordings were made in the presence of 0.5 mM glutathione to reduce the indole. In experiments without glutathione, the quenching was uniform over the entire field, and fluorescence traces were corrected by subtracting the time course of fluorescence change attributable to byproduct release detected in the region of the patch electrode where no Ca^{2+} change occurs. The contribution to the rate of change of bis-fura-2 fluorescence was found to be negligible and had no effect on estimates of Ca^{2+} flux.

Estimation of cytosolic Ca^{2+} flux. The concentration of Ca^{2+}-bound dye, D_{Ca}, when $D_{Ca} \gg Ca_f$, where Ca_f is the free [Ca^{2+}], is given by the following equation (Ogden and Capiod, 1997): $D_{Ca} = D_T \cdot (F_{min} - F)/(F_{min} - F_{max})$, where D_T is the total concentration of the dye; F is the fluorescence; and F_{min} and F_{max} are the fluorescence at zero and saturating [Ca^{2+}]. To obtain estimates of F_{min} and F_{max}, the ratios of bis-fura-2 fluorescence at 420 to that at 360 nm excitation (the isoemissive wavelength), R_{min} and R_{max}, respectively, were determined separately in the microscope at zero and saturating Ca_T immediately before measurements. F_{min} was calculated from the relation $F_{min} = F_{max} + (F_i - F_{max}) \cdot (R_{min} - R_{max})/(R_i - R_{max})$. At 420 nm excitation, F_{max} and $R_{max} = 0$ for bis-fura-2, giving $F_{min} = F_i \cdot R_{min}/R_i$. In $n = 9$ PNs, F_i/F_{min} was estimated to be 0.92 ± 0.04 (SEM) in distal dendritic regions, providing an estimate of the initial Ca_f of 32 nM, assuming $K_{(Ca)} = 370$ nM for bis-fura-2 (data from Molecular Probes). Net Ca^{2+} flux into the cytosol is proportional to the rate of change of D_{Ca} and, in conditions here, was estimated from

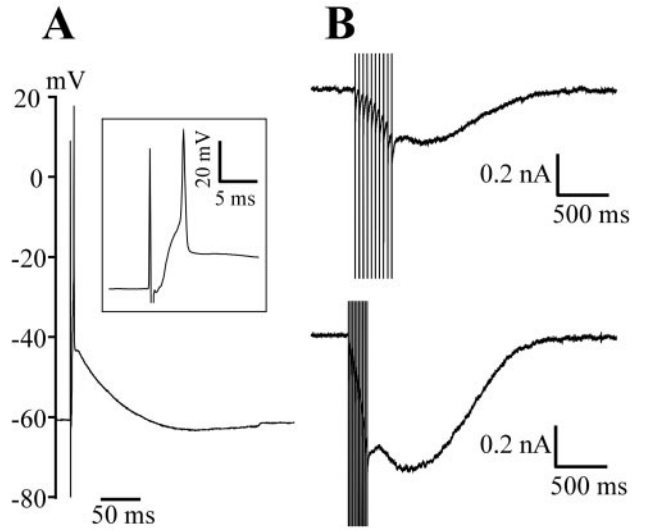

Figure 1. sEPSC evoked at low PF stimulation intensity, 20 d PN in a transverse slice, stimulation in the granule cell layer, 32°C. *A*, Current-clamp recording showing a single action potential evoked in PN by 25 μA 100 μsec stimulation at 1 Hz in the granule cell layer. No receptor antagonists are present. Inset, Action potential on a faster time scale. *B*, Same PN in voltage clamp, −67 mV, with 20 μM NBQX added to the bathing solution. Trains of stimuli at the same intensity as in *A* evoke an sEPSC with 10 pulses at 25 Hz (top) or 50 Hz (bottom) delivered every 10 sec.

the maximum rate of rise of $(F_i - F)/(F_i)$ for comparison with net ionic flux measured by the mGluR1 current.

Results

Stimulation requirements to elicit the sEPSC

It has been reported that the sEPSC requires very strong stimulation when evoked by local PF activation in sagittal slice orientation (Takechi et al., 1998), questioning the physiological importance of the sEPSP. Because sagittal orientation is not optimal for PF stimulation, the stimulus parameters required to evoke the sEPSC were tested here in 350 μm transverse cerebellar slices from 20-d-old rats. They were quantified in relation to the threshold stimulus at 1 Hz, which elicits a single PN somatic action potential (conditions: 32°C, GABA, and glutamate receptor antagonists absent). Diffuse activation of parallel fibers innervating the PN was made with extracellular stimulation in the granule cell layer, close to regions where PN soma were seen as a continuous layer with dendrites oriented downward into the slice. Once the threshold PF stimulation required to elicit a PN spike was found in current clamp, the slice was perfused with 20 μM NBQX to block AMPA receptors, eliminating the fast EPSP and action potential. The sEPSC was evoked in voltage clamp with PF stimulus trains of different frequency and duration at the same threshold intensity. Figure 1*A* shows the fast EPSP and superimposed spike of a PN evoked by threshold parallel fiber stimulation at 1 Hz. The slice was perfused with NBQX 20 μM for 5 min, monitoring the decline of the fast EPSP, and the recording switched to voltage clamp (holding potential, −67 mV) to record the current evoked by trains of stimuli at threshold intensity. sEPSCs, peaking in ~0.5 sec, were obtained with 10 pulses at frequencies of >20 Hz (Fig. 1*B*). The sEPSC was blocked reversibly by 1 mM MCPG (Hayashi et al., 1994) (data not shown; $n = 3$). This confirms that the mGluR-mediated sEPSC is readily evoked with trains of stimuli in the granule cell layer at threshold for excitation of the PN and does not require excessively high stimulation intensities or frequencies. In the experiments described below, the sEPSC was mimicked with fast application of glutamate by photolysis to activate mGluR1 independently of presynaptic stimulation, permitting pharmacological investigation of postsynaptic processes associated with Ca^{2+} metabolism.

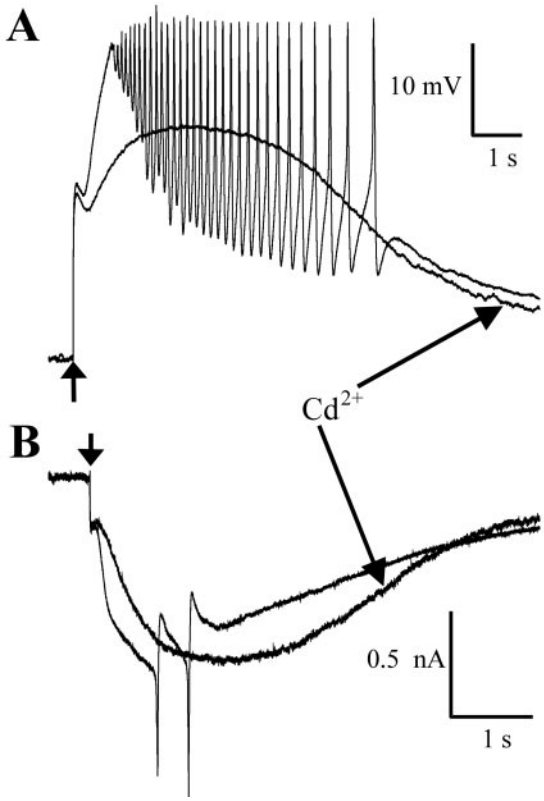

Figure 2. Contribution of voltage-gated Ca^{2+} channels to the rise of the mGluR1-evoked potential. Membrane potential change (*A*) and current at −75 mV (*B*) evoked by photolytic release of 70 μM L-glutamate from NI-caged glutamate in a 20 d PN before and after addition of 50 μM $CdCl_2$ are shown. NBQX (100 μM), AP-5 (50 μM), bicuculline (10 μM), and TTX (1 μM) are present.

Effect of Ca^{2+} channel antagonists on the mGluR1-evoked membrane potential change

The sEPSP or sEPSC evoked by tetanic PF stimulation is able to produce sufficient depolarization in the dendrites of PN to activate Ca^{2+} channels, producing slow regenerative action potentials (Batchelor et al., 1994). The contribution of Ca^{2+} channel activation to the potential change or current evoked by maximal mGluR1 activation was tested with photorelease of L-glutamate in 1 msec over the entire PN dendritic field in the presence or absence of Ca^{2+} channel blockers. Cd^{2+} (40–400 μM) and AGA4A toxin (0.2–1 μM) were found to prevent regenerative spiking and to slow the time course of the mGluR1-evoked potential or conductance. This is illustrated by the records in Figure 2, which show the abolition of spikes and the slowed rise time of membrane potential (Fig. 2*A*) or current (Fig. 2*B*) with 200 μM Cd^{2+} present. The results of eight experiments showed a slowing of the time to peak by 0.9 ± 0.35 sec (SEM) in the presence of Cd^{2+}. In similar experiments with 0.2–1 μM AGA4A, the time to peak current in AGA4A was slowed by 1.7 ± 0.52 sec ($n = 6$). Both sets of results indicate a contribution from voltage-gated Ca^{2+} channels to the current elicited by mGluR1 activation. This is not surprising even in voltage clamp if current arises from mGluR1 located in spines because the dendrites of 20 d PN are not adequately controlled. Activation of Ca^{2+} channels by den-

dritic depolarization would produce a widespread increase of intracellular [Ca^{2+}]. Ca^{2+} permeability of the mGluR1 channel, on the other hand, would provide a more specific and local signaling mechanism. Experiments described below to quantify Ca^{2+} influx through the channels activated by mGluR1 were made with voltage-gated Ca^{2+} channels blocked.

Intracellular [Ca^{2+}] increase associated with the mGluR1 sEPSP

The Ca^{2+} concentration changes associated with the mGluR1-mediated potential were investigated with the fluorescent Ca^{2+} indicator fluo-4. Ca^{2+} entry through Ca^{2+} channels activated by depolarization was blocked with AGA4A, and, to prevent contributions from inositol trisphosphate and diacylglycerol production after mGluR1 activation, the phospholipase C (PLC) pathway was inhibited with 2.5 or 5 μM U-73122. This compound is known to inhibit activation of PLCβ4 present in PN (Cruzblanca et al., 1998). The results in one cell are illustrated in Figure 3, *A* and *B*. The fluorescence change evoked by L-glutamate, computed as $\Delta F/F$, was monitored in the distal dendritic field in the region indicated in Figure 3*A*. It is displayed together with the membrane potential change recorded at the soma in Figure 3*B*. The fluorescence change in the distal dendrites and the membrane potential followed similar time courses. The effect of U-73122 on the Ca^{2+} signal and membrane potential was compared with controls in the same cell, and the data are summarized in Fig. 3*C*. U-73122 at 2.5 or 5 μM had no effect on the amplitude of mGluR1-mediated potential or on the $\Delta F/F$ Ca^{2+} signal in the distal dendrites.

The time course of $\Delta F/F$ in relation to peak membrane voltage (V_m) or conductance was analyzed in different regions of the PN in the absence of U-73122 with Ca^{2+} channels blocked. As shown in Figure 3*D*, the time courses were similar in the distal dendritic field, peak Ca^{2+} signal delayed by 156 ± 50 msec (SEM; $n = 9$) with respect to peak V_m. However, Ca^{2+} was further delayed with respect to the potential change in the proximal dendrites (745 ± 304 msec) and substantially in somatic regions (5296 ± 640 msec). The late, somatic Ca^{2+} signal was seen in 9 of 18 PNs tested at a low (30 μM) glutamate concentration in the absence of U-73122. Measurements in the presence of U-73122 were often later in the experiment when somatic fluorescence saturated the CCD. However, in six PNs in which the soma fluorescence was not saturating, a Ca^{2+} signal was seen in the dendrites but not the soma in the presence of U-73122. The results suggest that the delayed somatic Ca^{2+} signal is mediated by PLCβ and is most likely attributable to mGluR1-evoked Ca^{2+} release from stores. An earlier part of this study showed that extracellular naphthylacetyl spermine (NA-spermine) or the adamantane derivative [1-trimethylammonio-5-(1-adamantane-methylammoniopentane)dibromide] (IEM1460) (Magazanik et al., 1997) block the sEPSP channel (Ogden and Canepari, 2001). As shown in Fig. 3*E* for NA-spermine and Figure 4*D* for IEM1460, both prevented the fluorescence change in the distal dendrites after 10–20 min of incubation. It is of interest to know whether the Ca^{2+} influx into the cytosol is correlated quantitatively with the current through the mGluR1 channels, as demonstrated for ligand-gated Ca^{2+}-permeable cation channels elsewhere.

Ca^{2+} permeability of the mGluR1 channel

To obtain quantitative measurements of Ca^{2+} influx associated with the mGluR1 current, experiments were made with 1 mM bis-fura-2 and 100 μM Ca^{2+} added to the internal solution to impose a resting level of free Ca^{2+} close to 30 nM. The high concentration of bis-fura-2 provides the dominant Ca^{2+} buffer and permits the total Ca^{2+} concentration change to be monitored as the change in Ca^{2+}-bound indicator (see Materials and Methods). One micromolar AGA4A was present to block voltage-activated Ca^{2+} channels, and 5 μM U-73122 was present to inhibit PLCβ to prevent mGluR1-mediated release from stores. In a first set of experiments ($n = 6$), images were acquired with an intensified CCD camera. Figure 4*A* shows a fluorescence image of a PN filled from the patch pipette with 1 mM bis-fura-2. L-Glutamate (112 μM) was released over the soma and dendritic tree to produce maximal activation of mGluR1 receptors (Cane-

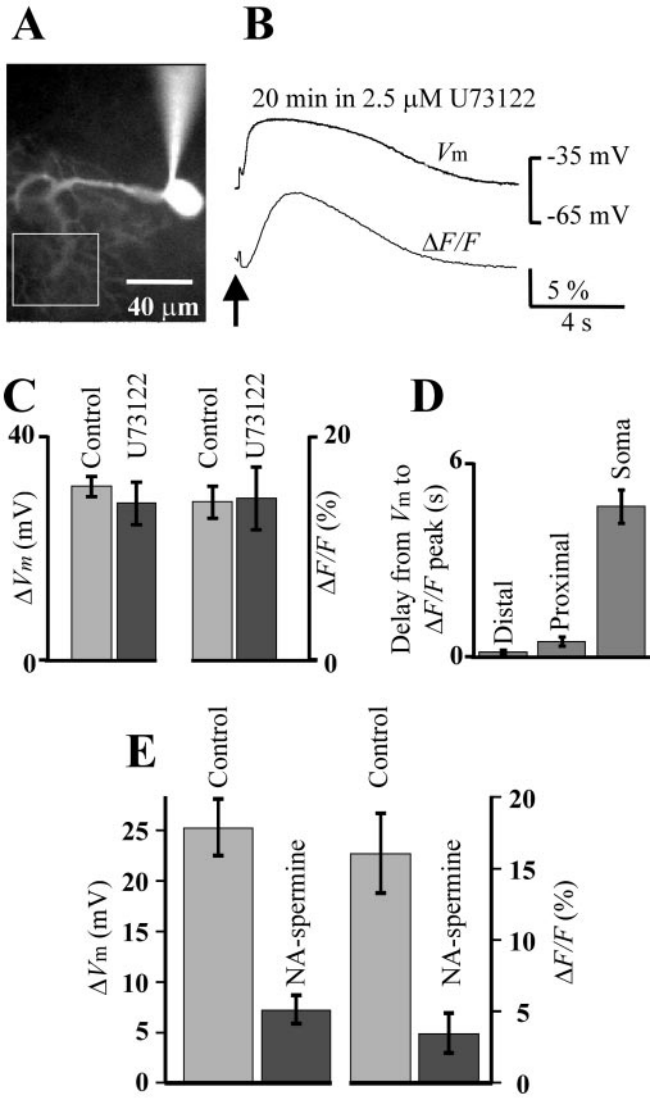

Figure 3. Intracellular [Ca^{2+}] increase associated with the sEPSP. *A*, Fluorescence image from a PN loaded with 500 μM fluo-4. The external solution contained NBQX (100 μM), AP-5 (50 μM), bicuculline (10 μM), TTX (1 μM), and AGA4A (1 μM). *B*, Membrane potential change (top trace) and fractional change in calcium fluorescence ($\Delta F/F$; bottom trace) in the square region (distal dendrite) depicted in *A* evoked by photolytic release of 70 μM L-glutamate from NI-caged glutamate 20 min after the addition of 2.5 μM U-73122. *C*, Mean and SEM (5 cells) of the peak membrane potential change (left histogram) and the peak calcium fluorescence change (in the distal dendrite; right) in control conditions or 20 min after addition of 2.5 μM U-73122. *D*, Mean and SEM (9 cells) of the delay (in seconds) between the peak of the membrane potential and the peak of the fractional change in calcium fluorescence in the distal dendrite (>100 μm from the soma), in the proximal dendrite, and in the soma. U-73122 is absent. *E*, Mean and SEM (6 cells) of the peak membrane potential change (left) and of the peak fluorescence change $\Delta F/F$ in the distal dendrite (right) in control conditions or 20 min after addition of 100 μM NA-spermine.

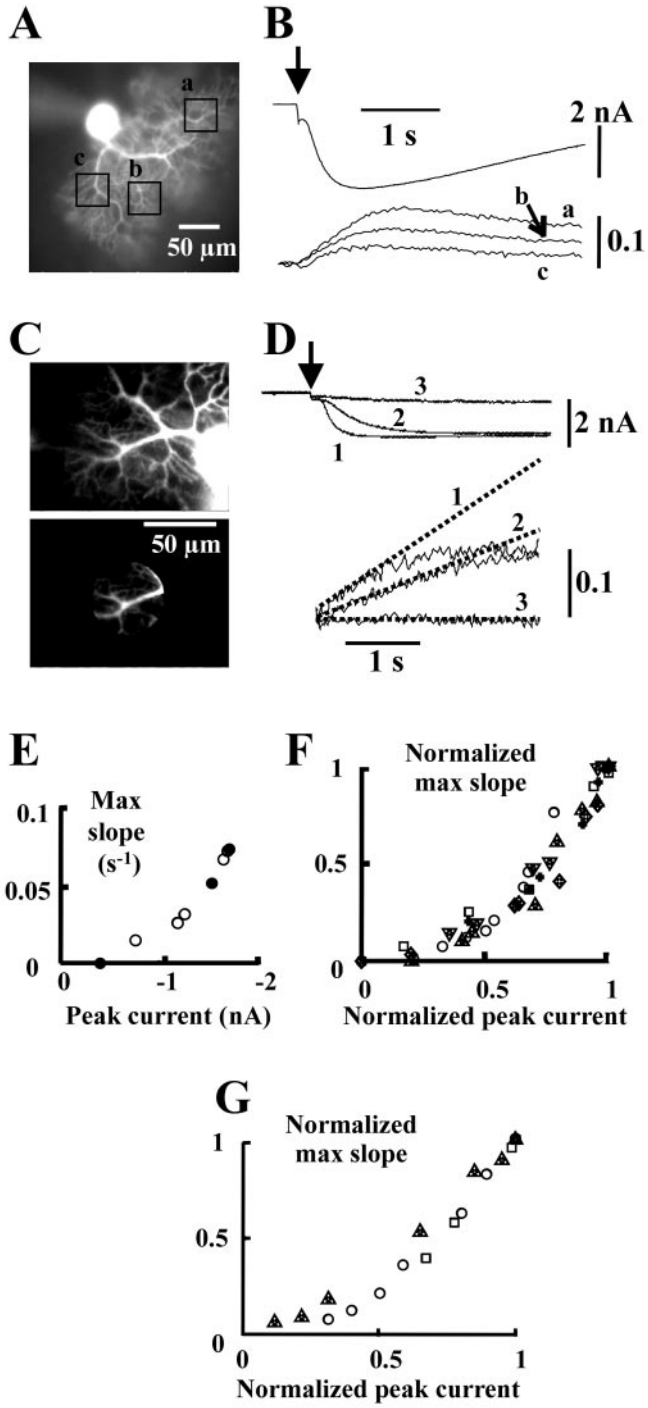

Figure 4. Quantitative estimation of Ca^{2+} influx during the mGluR1-activated current. *A*, Fluorescence image from a PN loaded with 1 mM bis-fura-2 recorded with the intensified CCD camera. *B*, mGluR1 current at −75 mV (top trace) evoked by release of 112 μM L-glutamate and corresponding fluorescence changes, $(F_i - F)/F_i$ (bottom traces a–c), in the regions (a–c) indicated in *A*. The timing of the flash is indicated by the arrow. $(F_i - F)/F_i$ traces were corrected for the loss of fluorescence attributable to the byproduct release (see Materials and Methods). *C*, Fluorescence from a PN loaded with 1 mM bis-fura-2 (top) and region of PMT recording in the dendrites (bottom). *D*, Time course of mGluR1 currents (top traces 1–3) and of the corresponding $(F_i - F)/F_i$ (bottom traces 1–3) recorded with the PMT in the region indicated in *C*. Recordings were done 0 (1), 9 (2), and 21 (3) min after the addition of 250 μM IEM1460 to the external solution. The arrow indicates the timing of the flash releasing 112 μM L-glutamate. The control solution contained 0.5 mM glutathione, and no correction was made to fluorescence data. *E*, Plot of the maximum rate of change of total Ca^{2+} $D_{Ca} = (F_i - F)/F_i$ against the peak mGluR1 current for the PN shown in *C*. Filled circles are data from *D*. *F*, Plot of the maximum rate of change of $(F_i - F)/F_i$ against the peak mGluR1 current for six PNs in which progressive block of the mGluR1 current and of the bis-fura-2 fluorescence signal was obtained either with 250 μM IEM1460 ($n = 5$) or with 300 μM rimantidine ($n = 1$). Both currents and $(F_i - F)/F_i$ slopes were normalized to the control in each cell. Each PN is represented by a different symbol. *G*, Maximum rate of change of $(F_i - F)/F_i$ plotted against the peak mGluR1 current for three cells without U-73122. Normalized data; mGluR1 current was progressively blocked with 250 μM IEM1460.

pari and Ogden, 2003). An inward current with peak amplitude of −2 nA was recorded at the soma, and the total Ca^{2+} concentration increase was monitored by the fluorescence change $(F_i - F)/F_i$ in three different regions of the distal dendritic tree, indicated by a–c in Figure 4*A*. The three regions gave different amplitudes of $[Ca^{2+}]$ change, but each had a time course similar to that of the whole-cell mGluR1 current (Fig. 4*B*). Because glutamate release was spatially uniform and complete in 1 msec, the differences in amplitude in the three regions must be attributable to nonuniform properties of the dendrites, possibly the mGluR1 current density or the ability of the dendrites to sequester Ca^{2+}. In three PNs where the peak inward current was <1 nA, no bis-fura-2 fluorescence change was detected. In three other PNs with peak inward current of >1.5 nA, signals with $(F_i - F)/F_i$ ranging between 0.01 and 0.25 were recorded in different regions of the distal dendritic tree. Assuming that the concentration of bis-fura-2, D_T, is equal to the pipette concentration of 1 mM, the magnitude of the total Ca^{2+} concentration change can be calibrated, $(F_i - F)/F_i = 0.1$ corresponding approximately to a total $[Ca^{2+}]$ change of 100 μM.

To improve the signal/noise ratio and to minimize photobleaching, a second set of experiments was done with a photomultiplier tube recording fluorescence from a circular region of 50 μm diameter in the distal dendrites (see Materials and Methods). In the presence of 1 μM AGA4A and 5 μM U-73122, the mean peak current and the peak values of $(F_i - F)/F_i$ in 13 PNs after photorelease of 60 or 120 μM L-glutamate were -1.41 ± 0.17 nA and 0.067 ± 0.017, respectively (SEM; $n = 13$). In 2 of 20 PNs, no Ca^{2+} signal was resolved in the region selected.

If the increase in $[Ca^{2+}]$ recorded with bis-fura-2 is attributable to Ca^{2+} influx through the mGluR1-activated channels, then a correlation is expected between the net flux, measured as rate of change of total $[Ca^{2+}]$, and the mGluR1 current. Ca^{2+} influx was estimated by measuring the maximum slope of $(F_i - F)/F_i$. Activation of mGluR1 was maximal, and the channels were progressively blocked with the pore-blocking adamantane derivatives rimantadine and IEM1460, ligands that produce a use-dependent, reversible block of the mGluR1 current (Ogden and Canepari, 2001). Figure 4*C* shows the region selected for recording in the dendritic tree of a PN. Flashes releasing 112 μM L-glutamate were given in pairs separated by 30 sec every 3 min after addition of 250 μM IEM1460 to the bath. Three recordings (0, 9, and 21 min after IEM1460 addition; records 1–3) are shown in Figure 4*D*. The top traces are membrane current, and the bottom traces are $(F_i - F)/F_i$ calculated from fluorescence signals. The maximum rate of change of total $[Ca^{2+}]$ is indicated by the lines drawn to the data. The maximum slope in each fluorescence record corresponded in time with the peak mGluR1 current, within the constraints of the signal/noise ratio, and both progressively decreased in amplitude with IEM1460 exposure. Some recovery of mGluR1 current occurred between pairs of pulses, permitting acquisition of a range of amplitudes in each cell at maximal mGluR1 activation. Figure 4*E* shows a plot of the maximum slope of $(F_i - F)/F_i$ against the mGluR1 peak current for eight recordings in this cell. There is a correlation between the

←

current amplitude and the rate of Ca^{2+} concentration increase, as expected if a proportion of current is carried by Ca^{2+} ions. Similar results were obtained in a further five cells in which the block was obtained either with 250 μM IEM1460 or with 300 μM rimantidine. Figure 4*F* shows the maximum slope of $(F_i - F)/F_i$ plotted against the mGluR1 peak current, both sets of data normalized to control amplitude in each cell ($n = 6$ PNs). The data show that with uniform maximal activation of mGluR1 receptors, the Ca^{2+} flux into the cytosol is strongly correlated with the ion flux measured by the amplitude of mGluR1 current. Furthermore, there is no detectable Ca^{2+} concentration change at low mGluR1 current amplitudes, indicating that there is no cytosolic release of Ca^{2+} from stores in these conditions. The supralinear relation between net influx and mGluR1 current may be explained by the simultaneous loss of fluorescence attributable to Ca^{2+} extrusion, which will have a greater effect on the net flux at low levels of influx if the extrusion mechanisms show saturation.

In seven PNs, the correlation was tested in the absence of U-73122 during block by 250 μM IEM1460 ($n = 3$; Fig. 4*G*) or 1 mM rimantidine ($n = 4$). In these conditions, the results were similar. In the distal dendrites, the fluorescence signal was abolished when the current was reduced to low levels, showing no evidence of store-released Ca^{2+} at high levels of mGluR1 activation. Data described above in connection with Figure 3*D* showed slow increases in somatic $[Ca^{2+}]$ at a low glutamate concentration in 50% of PNs in the absence of U-73122, which were abolished in the presence of U-73122, suggesting that the slow somatic increase is PLCβ-mediated Ca^{2+} release from stores. To test whether the high glutamate concentration used in Figure 4*G* may have prevented Ca^{2+} release from stores, bis-fura 2 fluorescence from a circular region of 50 μm diameter centered on the soma was recorded in nine cells soon after whole-cell recording. Four concentrations of L-glutamate were photoreleased on each cell: 13, 35, 53, and 112 μM. A $[Ca^{2+}]$ increase, peaking 5–10 sec after the flash and similar to that observed in the experiments with fluo-4 (Fig. 3*D*), was detected in four of nine cells at 13 μM glutamate, in three of nine cells at 35 μM glutamate, and in one of nine cells at higher concentrations of glutamate. Furthermore, in two cells, the calcium signals at low glutamate concentrations were blocked by subsequent bath application of 5 μM U-73122. These results indicate that Ca^{2+} release from stores may occur only at low glutamate concentrations but is suppressed at the maximal concentrations applied in experiments shown in Figure 4*E–G*.

The possibility still exists that the Ca^{2+} influx occurred through voltage-gated channels that were not blocked by AGA4A and were activated by the loss of dendritic voltage clamp (voltage escape) during large mGluR1 currents. This was tested in two PN in which the pipette potential was depolarized to –10 mV to produce a dendritic potential in the absence of glutamate similar to the dendritic depolarization attributable to voltage escape during the mGluR1 current. The bis-fura-2 fluorescence changes evoked by depolarization were compared with those at –75 mV attributable to 112 μM L-glutamate, with AGA4A (1 μM) and U-73122 (5 μM) present. In the first cell, the current induced at –10 mV was +2.5 nA, and the resulting membrane potential at the distal dendrite was calculated as −45 mV on the basis of the two-compartment model for electrotonic potential in the dendrites (see Materials and Methods; total dendrite + series resistance, 14 MΩ). This depolarization produced a very small change in fluorescence with a maximum rate of change of $(F_i - F)/F_i$ of <0.002/sec. In the same cell at –75 mV, an mGluR1 current of −0.8 nA, driving the distal dendrite to a calculated potential of −63 mV, generated a larger fluorescence change with a maximum $(F_i - F)/F_i$ slope of 0.03/sec. In the other cell, the current at –10 mV of +2 nA gave a calculated dendritic depolarization to −46 mV. This was associated with a rate of change of bis-fura-2 fluorescence of 0.005/sec. In the same cell, at –75 mV, an mGluR1 current of −1 nA, driving the distal dendrite to a calculated potential of –57 mV, generated a fluorescence change with a maximum $(F_i - F)/F_i$ slope of 0.08/sec. This comparison indicates that, in the presence of AGA4A, there was negligible contribution from activation of voltage-gated Ca^{2+} channels to the change of bis-fura-2 fluorescence during the mGluR1 current. Thus, the results with Ca^{2+} indicators show that Ca^{2+} influx during the mGluR1 current occurs through mGluR1-activated channels. However, the Ca^{2+} permeability of the mGluR1 channels relative to Na^+ cannot be calculated because the relative membrane areas for current and Ca^{2+} flux are not known.

Single-channel conductance and open probability of the sEPSP mGluR1 channel

The mGluR1-activated conductance increase has been shown previously to be associated with an increase in membrane current fluctuations ("noise") seen with high-gain bandpass recording (Canepari et al., 2001b). This provides evidence of high turnover in ion permeation, characteristic of a channel rather than an electrogenic transporter, and was seen with photolytically released L-glutamate (with ionotropic receptors blocked) and with the selective mGluR1 agonist DHPG (Canepari et al., 2001b). Here, the unitary current and open probability of the sEPSC channel were investigated further with direct postsynaptic mGluR1 activation by photolysis, with bath application of DHPG, and with parallel fiber or climbing fiber stimulation.

Single-channel current during sEPSC evoked by photolytic release of L-glutamate

The mean current and high-gain bandpass-filtered current evoked by photorelease of 60 μM L-glutamate on a PN voltage clamped at –75 mV are shown in Figure 5*A*. Records were obtained with ionotropic receptors, Na^+ and Ca^{2+} channels blocked. The bandpass records were obtained by reversing the DC records in time and applying a Butterworth eight-pole characteristic, usually 2–100 Hz (−3 dB), thus avoiding high-pass ringing attributable to the initial, fast-rising transporter current. The variance was calculated in 0.5-sec-long segments of data from the bandpass records and plotted against the corresponding mean current in that segment. A plot of variance, *var*, against time is shown in Figure 5*B*, and a plot of *var* against mean current, I^* (without subtraction of holding current), is shown in Figure 5*C*. An estimate of the single-channel current can be obtained from the initial slope of the relation $var(I) = i \cdot I^* \cdot (1 - p)$, where $var(I)$ is the current variance; I^* is the mean current in each data segment; i is the single-channel current, and p is the open probability. Linear regression to estimate the initial slope was applied to data points within the range of mean current I^* positive to −600 pA to avoid errors attributable to depolarization of the distal dendrites and consequent loss of driving potential of >10 mV, based on values for series resistances derived from cable analysis (see Materials and Methods). Fits were constrained to the baseline variance and current. The initial slopes were in the range of –10 to –74 fA. The noise increase during the mGluR1 current can arise directly from the activated channels. It can, however, arise indirectly, for instance, through hyperpolarization-activated channels (I_H) or Ca^{2+} activation of K^+ channels after

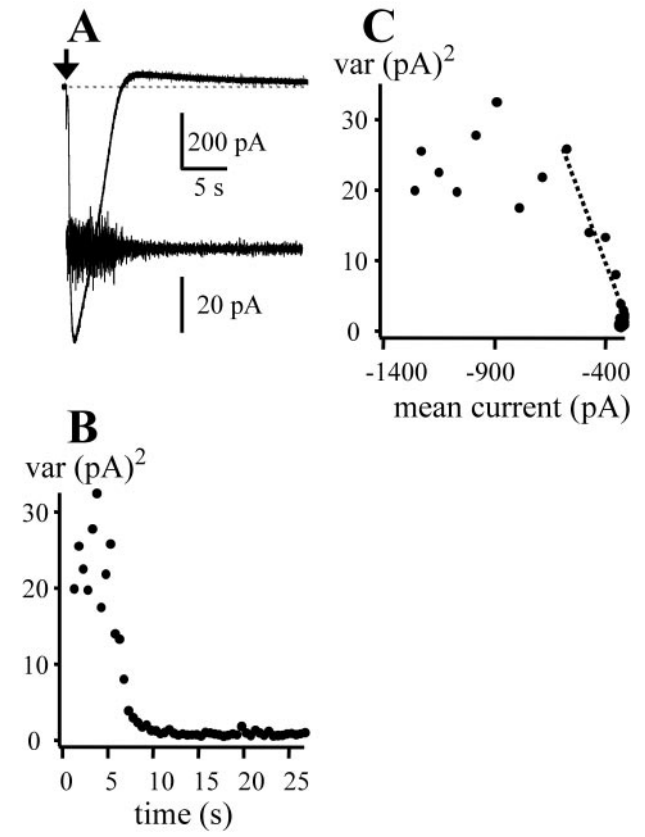

Figure 5. Fluctuation analysis of the mGluR1 current, Purkinje neuron, 21 d, voltage clamp, –75 mV, 32°C. One hundred micromolar NBQX, 1 μM TTX, and 1 μM AGA4A were present in the external solution. *A*, Current activated by 56 μM L-glutamate released at the time indicated by the arrow. Low-gain DC 2 kHz and high-gain bandpass records (2–100 Hz, −3 dB, 8-pole Butterworth) are shown. *B*, Variance calculated in 0.5 sec segments of the bandpass record. *C*, Variance in 0.5 sec segments plotted against mean current. Linear regression constrained to the baseline variance and current gives an initial slope of –74 fA.

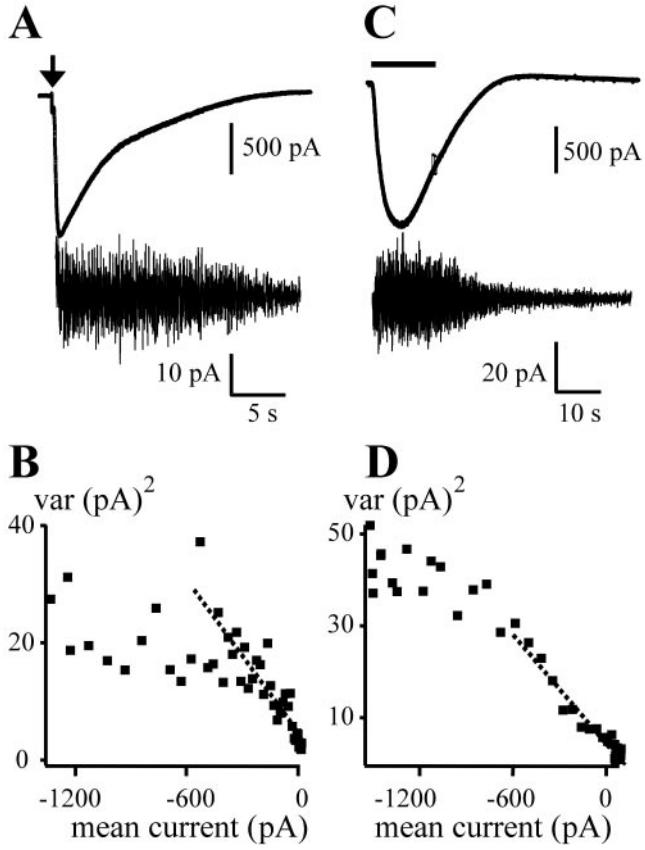

Figure 6. Fluctuation analysis of the mGluR1 current with K channels and I_H blocked, Purkinje neuron, voltage clamp, –75 mV, 32°C. *A*, Current activated by 56 μM L-glutamate released at the time indicated by the arrow. A low-gain DC 2 kHz and high-gain bandpass records (2–100 Hz, −3 dB, 8-pole Butterworth) are shown. *B*, Plot of the variance against mean current in 0.5 sec data segments. Initial slope, –38 fA. *C*, Same PN as in *A* and *B*. Activation of mGluR1 receptors by bath perfusion of 100 μM DHPG during the time indicated by the bar. Low-gain DC and high-gain bandpass records (1–100 Hz, −3 dB) are shown. *D*, Plot of variance against mean current evoked by DHPG, 1 sec data segments; initial slope, – 42 fA.

Ca^{2+} entry or release. To test these possibilities, a set of experiments was done in the presence of paxilline (10 μM; Womack and Khodakhah, 2002) or TEA (1 mM) to block large-conductance K^+ channels, dequalinium (10 μM) or apamin (1 μM) to block small-conductance SK potassium channels (Cingolani et al., 2002), inhibitors found here to block the afterhyperpolarizing current in PN, and 4-ethylphenylamino-1,2-dimethyl-6-methylaminopyrimidinium chloride (10 or 20 μM), shown to inhibit I_H in PN (Canepari et al., 2001b). The results are illustrated in Figure 6, *A* and *B*. The noise increase remains, coincident with the peak inward current, as in the absence of K^+ channel blockers (compare with Fig. 5*A*). In 14 experiments, the mean unitary current was –22 ± 4.5 (SEM) fA at –75 mV. Results reported earlier (Canepari et al., 2001b) showed a reversal potential close to zero for the mGluR1-evoked conductance and a linear current–voltage relation. The single-channel conductance calculated from these data with a driving potential of −75 mV gives a mean of 0.29 ± 0.06 (SEM) pS.

Selective mGluR1 agonist DHPG

For comparison with glutamate-evoked current, the single-channel current evoked by bath application of the selective mGluR1/mGluR5 agonist DHPG (100 μM) was also determined in six experiments. The results with DHPG in the presence of K^+ channel and I_H blockers are illustrated in Figure 6, *C* and *D*. In six PNs from 20 d rats at –75 mV, the single-channel current during the rising phase of the DHPG response was estimated at –19.3 ± 6.0 (SEM) fA ($n = 6$) compared with –18.3 ± 5.5 fA ($n = 6$) in the same PNs activated by photoreleased L-glutamate.

Single-channel current during the PF or CF evoked sEPSC

The sEPSC evoked by PF stimulation was analyzed in the same way to obtain an estimate of the single-channel current. The sEPSCs, obtained with 10 μM NBQX present in PN of rats aged 14–20 d, were bandpass-filtered at 5–100 Hz (−3 dB), and the variance in 0.2 sec samples was plotted against the mean current. The results obtained with tetanic PF stimulation, 5 or 10 pulses at 100 Hz, are illustrated in Figure 7, which shows an increase of current noise coinciding with the peak sEPSC. In seven PNs, the average single-channel current at –75 mV estimated from the initial slope of variance–mean current plots was $i = -39 \pm 5.3$ (SEM) fA. The sEPSC evoked by climbing fiber stimulation in the presence of NBQX (10 μM) and glutamate uptake inhibitor DL-threo-β-Benzyloxyaspartic acid (100 μM) gave a unitary current of $i = -37$ fA.

Influence of dendritic filtering on the estimate of single-channel current

The current variance recorded at the soma arising from distal mGluR1 channels is expected to be attenuated by low-pass filtering in the dendrites, and, consequently, the single-channel con-

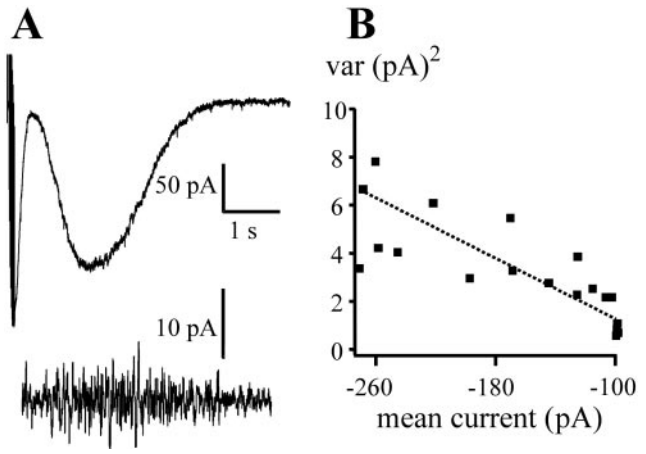

Figure 7. Fluctuation analysis of sEPSC evoked by PF stimulation. sEPSC was evoked by 10 pulses at 100 Hz, 60 V, and 100 μsec in the molecular layer of a transverse slice from a 16 d rat cerebellum, –70 mV, 25°C. The external solution contained 10 μM NBQX. The internal solution contained K gluconate with 0.5 mM EGTA and 1 mM *N*-(2,6-Dimethylphenylcarbamoylmethyl)triethylammonium bromide. A, Mean current DC 2 kHz and high-gain bandpass 5–100 Hz (−3 dB, 8-pole Butterworth) records. *B*, Plot of variance in 200 msec segments of data against the mean current. The fitted regression line constrained to baseline has a slope of –31 fA.

ductance may be underestimated. The influence of dendritic filtering was studied in 13- and 20-d-old rats. The dendritic tree of PN is much smaller at 13 d, and the reduced dendritic filtering might give a better estimate of the variance and single-channel current. In the two groups of data, the variance–mean relation with a 2–100 Hz recording bandwidth gave initial slopes of -18.0 ± 5.5 (SEM) fA ($n = 6$ PNs) at 20 d of age, similar to the value reported above, and -54.0 ± 8.2 fA ($n = 5$) at 13 d of age. These values are consistent with reduced PN dendritic filtering in 13- compared with 20-d-old animals. Spectral density of the variance and electrotonic parameters were compared for the two ages. This analysis is approximate and assumes a uniform distribution of active channels in the distal dendrites.

The slow time constants, τ, of the membrane-charging curves after +5 mV voltage steps from –75 mV were used to estimate half-power frequency, $f_c = 1/2\pi\tau$, of single-pole low-pass filtering by the dendrites (sampled a 250 kHz, low-pass-filtered at 50 kHz, –3 dB, in the presence of the I_H inhibitor ZD7288 10 μM). In PN from 20 d animals the mean was $\tau = 18.5 \pm 1.3$ msec, corresponding to mean $f_c = 8.6$ Hz. In 13 d animals, low-pass filtering was less: mean $\tau = 7.4 \pm 0.85$ msec, and $f_c = 21.5$ Hz. The spectral densities of the mGluR1 variance at 13 d had half-power frequencies lower than this, with mean of 10.8 Hz, indicating that in 13 d PN, most of the variance arising in the dendrites would be seen. The variance data from three 13 d PNs were reanalyzed with additional low-pass filtering imposed to mimic the additional dendritic filtering expected in 20 d PN, with $f_c = 9.8$ Hz. The variance–mean current relations gave new estimates of the single-channel current from the initial slopes, which now averaged –27 fA, attenuated by a factor of 0.5 ± 0.17 (mean ± SD) from the recorded mean of –54 fA at 13 d. Comparison of the filtered 13 d current of –27 fA with the value of –18 fA determined directly in 20 d animals indicates that dendritic filtering accounts for most of the difference in single-channel current between 20 and 13 d PN. The estimate of single-channel conductance for the mGluR1-activated channel of 0.29 pS obtained directly in 20 d animals is therefore underestimated by dendritic low-pass filtering, the factor of 0.5 obtained above giving 0.58 pS as an estimate for the mGluR1 single-channel corrected conductance in 20 d PN, similar to the uncorrected conductance of 0.72 pS at 13 d.

Thus, the unitary currents through mGluR1-activated channels evoked by synaptically released glutamate during PF or CF sEPSCs, by photoreleased glutamate, or by selective agonist DHPG are of similar small amplitudes and can be attributed to the mGluR1-activated nonselective cation channel. Taking a reversal potential close to 0 mV (Canepari et al., 2001b), the results indicate that an ion channel of sub-picoseiman conductance mediates the sEPSC and the glutamate- and DHPG-evoked mGluR1 currents.

Power spectra were calculated for mGluR1-evoked current in 13 d PN and corrected for low-pass filtering in the dendrites (Ogden and Colquhoun, 1986, their Appendix 1), giving a mean time constant of 12.7 msec for the main kinetic parameter of channel activation.

Open probability

A parabolic relation is predicted between variance $var(I)$ and mean current I^* (where $I^* = N \cdot p \cdot i$, with N the number of channels present, p the open probability, and i the single-channel current) as p increases between 0 and 1. In all cases recorded at high glutamate concentration or with DHPG, plots of variance–mean showed reduced slopes at large inward currents. This effect can be seen in Figures 5*C* and 6, *B* and *D*. The reduced slope could be attributable to either an increase of p to values approaching 0.5, or, if the mGluR1 current originates mainly in the distal dendrites, to a decrease of the driving potential as a result of dendritic depolarization produced by current flow through the dendrite and series resistances. To test whether the latter explanation could account for the sublinearity of variance–mean relations seen here, the linear electrotonic properties of each PN were investigated with rectangular voltage-clamp pulses (digitized at 250 kHz; low-pass filter, 50 kHz; –3 dB). A two-compartment approximation (Llano et al., 1991; Roth and Hausser, 2001) was used for the distribution of somatic and dendritic capacitance to obtain estimates of the series resistances from pipette to soma and from soma to distal dendrites. The potential drop, ΔV, between the distal compartment and the pipette as a result of current flow in the dendritic and series resistances was calculated for the mean current in each data segment. The fractional change of driving potential for ion channel current in the dendrites, $1 - \Delta V/E$, where E is the voltage-clamped pipette potential, was used to calculate the change of single-channel current expected due to the distal depolarization. Calculations assumed the reversal potential for single-channel current at 0 mV (Canepari et al., 2001b) and a linear channel conductance. The channel current, i, contributes as i^2 to the variance, $var(I) = i^2 \cdot N \cdot p \cdot (1 - p)$, and linearly to the mean current, $I^* = Npi$. This correction was applied to calculations of *var* and *mean* in the data of Figure 8*A* for glutamate-evoked current and Figure 8*B* for DHPG-evoked current in the same PN, with resistances of 7.4 MΩ for pipette to soma and 11.6 MΩ for soma to dendrites. The open circles are the uncorrected data, and the filled circles are the corrected data. The corrected plots of variance against mean current now show no systematic deviation from a straight line over the whole of the range of mean current. This suggests that the sublinear relation apparent in the raw data (open circles) of Figure 8, *A* and *B*, can be accounted for by mGluR1 current flowing through the pipette–soma and dendritic resistances in series. Similar calculations made in six PNs (20 d) with pipette–soma resistances ranging between 5.8 and 12.5 MΩ (mean, 8.7 MΩ) and soma–dendritic resistances of 5.0–15.2 MΩ resulted in lin-

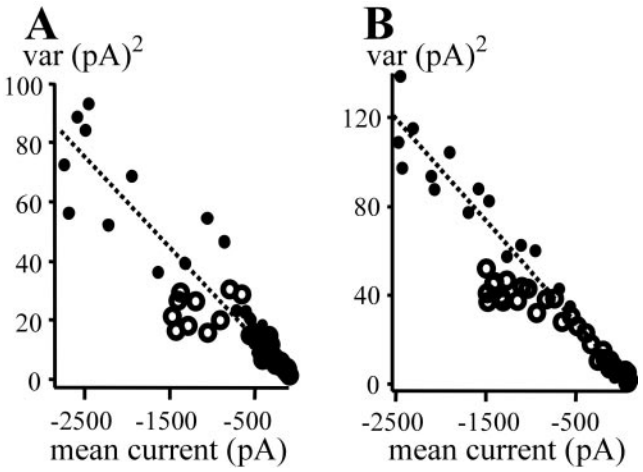

Figure 8. Low open probability of maximally activated mGluR1 current. *A*, Plot of variance against mean current for a 20 d PN activated by 112 μM L-glutamate. The external solution contained 100 μM NBQX, 1 μM TTX, 1 μM AGA4A, 20 μM ZD7288, 10 μM paxilline, and1 μM apamin. Data are shown without correction (open symbols) and after correction (filled symbols) for the effects of depolarization in the distal dendrites. Dendritic cable and pipette–soma series resistances are 17 and 6 MΩ, respectively. The fitted line has a slope of –31 fA. *B*, Plot of variance against mean current for a 21 d PN activated by 100 μM DHPG. Solutions are as in *A*. Data are shown without correction (open symbols) and after correction (filled symbols) for the effects of depolarization in the distal dendrites. Dendritic cable and pipette–soma series resistances are 11.6 and 7.4 MΩ, respectively. The fitted line has a slope of – 45 fA.

ear variance–mean current relations over the whole range. Thus, deviations from a linear relation in the raw data at a large inward current can be accounted for by the loss of driving potential in the series resistances. Furthermore, the linearity of corrected variance–mean current relations indicates that open probability is small, $p < 0.5$, even at maximal activation of the mGluR1 current used here.

Discussion

Properties of the sEPSP channel

The properties of the ion channel underlying the sEPSP determined by noise analysis provide information concerning the activation and identity of the channel. The results are consistent with a small, sub-picoseiman-conductance, nonselective cation channel that has a low open probability even when maximally activated by photoreleased L-glutamate or by the selective mGluR1 agonist DHPG. The open probability was also low during the PF evoked sEPSC; the sEPSC amplitudes seen during synaptic activation at 100 Hz were 5–10 times smaller than the maximal activation by photoreleased L-glutamate. The low open probability would allow large changes in the efficiency of excitation via mGluR1. This might happen during modulation by intracellular free Ca^{2+} concentration via CF activation, as suggested by Batchelor and Garthwaite (1997) and Dzubay and Otis (2002), or by modulation of pathways acting through tyrosine kinase and phosphatase, as suggested by Canepari and Ogden (2003). The functional significance of the potential modulatory pathways has not been established.

The single-channel properties estimated with noise analysis were similar when excitation was initiated by PF or CF stimulation, by photoreleased L-glutamate, or with the mGluR1 agonist DHPG. However, the single-channel currents estimated with PF stimulation were larger by a factor of 2, although still in the subpicoseiman range. Although it is possible that there is a difference between synaptic and extrasynaptic mGluR1 channels, it is unlikely that they are of different identity because they share unusual pharmacology (Ogden and Canepari, 2001), and the difference may be attributable to less dendritic filtering in the younger animals used for PF experiments.

The unitary conductance, of 0.29 pS estimated from the raw data and 0.58 pS when corrected for dendritic filtering, is small in the range of cation channel conductances. The sub-picoseiman conductance, linearity (Canepari et al., 2001b), Ca^{2+} permeability, and pharmacology of the pore block should help identify the molecular nature of the underlying channel.

It was reported recently that the mGluR1 current is reduced by expression of nonpermeant mutated TRPC1 channels in PN in slice culture and by 1-[β-(3-(4-Methoxyphenyl)propoxy)-4-methoxyphenethyl]-1H-imidazole an inhibitor of transient receptor potential-like channel type 1 (TRPC1) channels in acute slices. Furthermore, coexpression of mGluR1 and TRPC1 in cell lines reconstituted a nonselective cation current (Kim et al., 2003). These results suggest that TRPC1 is the channel mediating the mGluR1 sEPSP and provide a mechanism of activation via Homer scaffold proteins. However, the single-channel conductance of TRPC1 has been reported as 16 pS (Zitt et al., 1996), compared with the estimate here for the sEPSC channel of 0.6 pS, much smaller and more than can be accounted for by known factors. Furthermore, Gd^{3+} ions are reported to block TRPC1 (Zitt et al., 1996) but have no effect on the mGluR1 current (100 μM internally and externally, Canepari et al., 2001b). Finally, ligands that act as open channel blockers in unedited glutamate channels block the current, as reported here and by Ogden and Canepari (2001). Further investigation of the pharmacology of the PN sEPSP in adult cerebellum and comparison with recombinant candidate channels may provide an explanation for these discrepancies.

Ca^{2+} influx through the sEPSP mGluR1 channel

The Ca^{2+} concentration increase in the distal dendrites during the mGluR1-evoked conductance has a component that is attributable to Ca^{2+} influx through the mGluR1 channels. In the present conditions, with voltage-gated Ca^{2+} channels blocked and PLCβ inhibited to prevent mGluR1-mediated intracellular release, the Ca^{2+} concentration increase was correlated closely in size and time course with the amplitude of the mGluR1 current. A systematic investigation of channel-blocking ligands made as part of this study (Ogden and Canepari, 2001) showed that the mGluR1 channel was blocked in a use-dependent way by cationic adamantane derivatives rimantadine and IEM1460 (Magazanik et al., 1997) or by the Joro toxin analog naphthylacetylspermine. Pore-blocking ligands were used to modify the amplitude of the mGluR1 current without changing the level of receptor activation, and the use-dependent properties permitted a wide range of current amplitudes to be tested in each PN. The Ca^{2+} influx was measured as the rate of increase of total (bound plus free) intracellular [Ca^{2+}], monitored with a high concentration of bis-fura-2 at constant internal free [Ca^{2+}]. A good correlation in amplitude and time was found between the net Ca^{2+} influx and the amplitude of the peak mGluR1 current, indicating that a fraction of the current is carried by Ca^{2+} ions. In the present experiments, it was not possible to determine the fractional transport number for Ca^{2+} for comparison with published values for other nonselective cation channels because of the different areas of membrane sampled by the electrical and optical recording. It has been reported that the amplitude of the sEPSP or sEPSC is increased when cytosolic Ca^{2+} concentration increases (Batchelor and Garthwaite, 1997; Dzubay and Otis, 2002), suggesting

that some regenerative action of Ca^{2+} influx amplifying the mGluR1 conductance might occur.

The mGluR1 potential or current recorded at the soma had a time course similar to the Ca^{2+} concentration changes in the distal dendrites but not the proximal dendrites or soma. If the Ca^{2+} change is attributable to influx, as suggested by the data presented here, then it can be concluded that the mGluR1 current originates mainly in the distal dendrites.

The slow, somatic Ca^{2+} signal was not seen in the presence of U-73122, whereas it was in 9 out of 18 PNs in its absence, suggesting that it is mediated by PLCβ- and most likely $InsP_3$-evoked Ca^{2+} release from stores. It was seen at low glutamate concentrations, <35 μM, but not at high concentrations in the same cell, suggesting that store release is suppressed at high mGluR1 activation. This provides an explanation for the failure to observe Ca^{2+} release from stores in the dendrites with complete current block by rimantadine or IEM 1460 in the absence of U-73122 (Fig. 4*G*), experiments done with maximal glutamate concentrations to ensure full activation of mGluR1. At a low glutamate concentration, it was seen only in 50% of cells, suggesting that other factors may also be involved. The direct influx of Ca^{2+} through sEPSP mGluR1 channels will occur selectively in repetitively active spines, providing input specificity that may be important in initiating or maintaining plasticity at PF → PN synapses. In contrast, because of the high cytosolic diffusion coefficient of $InsP_3$ relative to Ca^{2+} (Allbritton et al., 1992), release from stores by $InsP_3$ will have a wider area of action, as demonstrated in PN dendrites (Finch and Augustine, 1998). Similarly, signaling by diffusible extracellular mediators implicated in cerebellar plasticity, such as nitride oxide released from PF with tetanic stimulation (Casado et al., 2002), will lack specificity unless interacting with a process localized to single PF spines. The mGluR1 initiates signaling in pathways that diverge after Gq coupling, one activating PLC and the other the sEPSP, as indicated by results obtained in Gq-deficient (Hartmann et al., 2002) and PLCβ-deficient (Sugiyama et al., 1999) mice. The two pathways appear to have different functions. $InsP_3$-evoked Ca^{2+} release from intracellular stores, occurring via PLCβ, results in activation of an inhibitory K^+ current (Khodakhah and Ogden, 1995; Finch and Augustine, 1998) and may occur only at low levels of stimulation (Takechi et al., 1998). The mGluR1 conductance, on the other hand, is depolarizing and excitatory. Consistent with this, there was little evidence of activation of an inhibitory K^+ current during the excitatory mGluR1 current. There was no effect of inhibitors of K^+ channels on the mean current or variance of the net inward current evoked by mGluR1 activation, indicating that K^+ channels were not activated even at elevated Ca^{2+} concentrations associated with the mGluR1 current. In some experiments, for example, that shown in Figure 5, an outward current of small amplitude relative to the excitatory current was evident as an elevated baseline at the end of the response and in a small proportion of responses was associated with a small, late increase of current variance that may be attributable to K^+ channel activation. These observations indicate that Ca^{2+} activation of K^+ channels is suppressed during the mGluR1 sEPSC.

The mechanism of the divergence and segregation of the two mGluR1 pathways and the functional significance are not clear. It has been suggested that divergence results from αq coupling to PLCβ and coupling of $\beta\gamma$ to the sEPSP channel activation mechanism (Sugiyama et al., 1999). However, other points of interaction may be the suppression of $InsP_3$-evoked Ca^{2+} release by high cytosolic Ca^{2+} concentrations shown in PN (Khodakhah and Ogden, 1995) or by protein-tyrosine kinase and phosphatase signaling, demonstrated to be able to regulate the sEPSP (Canepari and Ogden, 2003). This type of modulation may enable one versus the other pathway. The results presented in Figure 1 show that the sEPSP can be evoked by low levels of tetanic PF stimulation, 10–100 Hz, at intensities that are threshold for PF excitation of the PN. PFs are thought to fire at frequencies as high as 1 kHz, sufficient to strongly activate the sEPSP. Although mGluR1s are strongly implicated in motor coordination, the role of the sEPSP and the associated Ca^{2+} influx in PN function remains to be clearly defined.

References

Aiba A, Kano M, Chen C, Stanton ME, Fox GD, Herrup K, Zwingman TA, Tonegawa S (1994) Deficient cerebellar long-term depression and impaired motor learning in mGluR1 mutant mice. Cell 79:377–388.

Allbritton A, Meyer T, Stryer L (1992) Range of messenger action of calcium ion and inositol 1,4,5 trisphosphate. Science 258:1812–1815.

Batchelor AM, Garthwaite J (1993) Novel synaptic potentials in cerebellar Purkinje cells: probable mediation by metabotropic glutamate receptors. Neuropharmacology 32:11–20.

Batchelor AM, Garthwaite J (1997) Frequency detection and temporally dispersed synaptic signal association through a metabotropic glutamate receptor pathway. Nature 385:74–77.

Batchelor AM, Madge DJ, Garthwaite J (1994) Synaptic activation of metabotropic glutamate receptors in the parallel fibre-Purkinje cell pathway in rat cerebellar slices. Neuroscience 63:911–915.

Canepari M, Ogden D (2003) Evidence for protein tyrosine phosphatase, tyrosine kinase, and G-protein regulation of the parallel fiber metabotropic slow EPSC of rat cerebellar Purkinje neurons. J Neurosci 23:4066–4071.

Canepari M, Nelson L, Papageorgiou G, Corrie JE, Ogden D (2001a) Photochemical and pharmacological evaluation of 7-nitroindolinyl- and 4-methoxy-7-nitroindolinyl-amino acids as novel, fast caged neurotransmitters. J Neurosci Methods 112:29–42.

Canepari M, Papageorgiou G, Corrie JE, Watkins C, Ogden D (2001b) The conductance underlying the parallel fibre slow EPSP in rat cerebellar Purkinje neurones studied with photolytic release of L-glutamate. J Physiol (Lond) 533:765–772.

Casado M, Isope P, Ascher P (2002) Involvement of presynaptic *N*-methyl-D-aspartate receptors in cerebellar long-term depression. Neuron 33:123–130.

Cingolani LA, Gymnopoulos M, Boccaccio A, Stocker M, Pedarzani P (2002) Developmental regulation of small-conductance Ca^{2+}-activated K^+ channel expression and function in rat Purkinje neurons. J Neurosci 22:4456–4467.

Cruzblanca H, Koh DS, Hille B (1998) Bradykinin inhibits M current via phospholipase C and Ca^{2+} release from IP3-sensitive Ca^{2+} stores in rat sympathetic neurons. Proc Natl Acad Sci USA 95:7151–7156.

Dzubay JA, Otis TS (2002) Climbing fiber activation of metabotropic glutamate receptors on cerebellar Purkinje neurons. Neuron 36:1159–1167.

Finch EA, Augustine GJ (1998) Local calcium signalling by inositol-1,4,5-trisphosphate in Purkinje cell dendrites. Nature 396:753–756.

Hartmann J, Blum R, Kovalchuk Y, Kuner R,. Durand GM, Miyata M, Kano M, Offermanns S, Konnerth A (2002) Gq dependence of mGluR-mediated synaptic signaling in cerebellar Purkinje cells. Soc Neurosci Abstr 339:15.

Hayashi Y, Sekiyama N, Nakanishi S, Jane DE, Sunter DC, Birse EF, Udvarhelyi PM, Watkins JC (1994) Analysis of agonist and antagonist activities of phenylglycine derivatives for different cloned metabotropic glutamate receptor subtypes. J Neurosci 14:3370–3377.

Hirono M, Konishi S, Yoshioka T (1998) Phospholipase C-independent group I metabotropic glutamate receptor-mediated inward current in mouse Purkinje cells. Biochem Biophys Res Commun 251:753–758.

Khodakhah K, Ogden D (1995) Fast activation and inactivation of inositol trisphosphate-evoked Ca^{2+} release in rat cerebellar Purkinje neurones. J Physiol (Lond) 487:343–358.

Kim SJ, Kim YS, Yuan JP, Petralia RS, Worley PF, Linden DJ (2003) Activation of the TRPC1 cation channel by metabotropic glutamate receptor mGluR1. Nature 426:285–291.

Llano I, Marty A, Armstrong C, Konnerth A (1991) Synaptic and agonist

induced excitatory currents of Purkinje cells in rat cerebellar slices. J Physiol (Lond) 434:183–213.

Magazanik LG, Buldakova SL, Samoilova MV, Gmiro VE, Mellor IR, Usherwood PN (1997) Block of open channels of recombinant AMPA receptors and native AMPA/kainate receptors by adamantane derivatives. J Physiol (Lond) 505:655–663.

Ogden D, Canepari M (2001) The cation channel underlying the slow EPSP in cerebellar Purkinje neurones is inhibited by pore blockers. Soc Neurosci Abstr 27:459.1.

Ogden D, Capiod T (1997) Regulation of Ca2+ release by InsP3 in single guinea pig hepatocytes and rat Purkinje neurons. J Gen Physiol 109:741–756.

Ogden DC, Colquhoun D (1986) Ion channel block by acetylcholine, carbachol and suberyldicholine at the frog neuromuscular junction. Proc R Soc Lond B Biol Sci 225:329–355.

Papageorgiou G, Corrie JET (2000) Effects of aromatic substituents on the photocleavage of 1-acyl-7-nitroindolines. Tetrahedron 56:8197–8205.

Roth A, Hausser M (2001) Compartmental models of rat cerebellar Purkinje cells based on simultaneous somatic and dendritic patch-clamp recordings. J Physiol (Lond) 535:445–472.

Sillevis-Smitt P, Kinoshita A, De Leeuw B, Moll W, Coesmans M, Jaarsma D, Henzen-Logmans S, Vecht C, De Zeeuw C, Sekiyama N, Nakanishi S, Shigemoto R (2000) Paraneoplastic cerebellar ataxia due to autoantibodies against a glutamate receptor. N Engl J Med 342:21–27.

Sugiyama T, Hirono M, Suzuki K, Nakamura Y, Aiba A, Nakamura K, Nakao K, Katsuki M, Yoshioka T (1999) Localization of phospholipase C beta isozymes in the mouse cerebellum. Biochem Biophys Res Comm 265:473–478.

Takechi H, Eilers J, Konnerth A (1998) A new class of synaptic response involving calcium release in dendritic spines. Nature 396:757–760.

Tempia F, Miniaci MC, Anchisi D, Strata P (1998) Postsynaptic current mediated by metabotropic glutamate receptors in cerebellar Purkinje cells. J Neurophysiol 80:520–528.

Womack MD, Khodakhah K (2002) Characterization of large conductance Ca2+-activated K+ channels in cerebellar Purkinje neurons. Eur J Neurosci 16:1214–1222

Zitt C, Zobel A, Obukhov AG, Harteneck C, Kalkbrenner F, Luckhoff A, Schultz G (1996) Cloning and functional expression of a human Ca2+-permeable cation channel activated by calcium store depletion. Neuron 16:1189–1196.